

# Experimental Performance of Concrete Columns with Composite Jackets under Blast Loading

By Tonatiuh Rodriguez-Nikl,<sup>1</sup> M.ASCE, Ph.D., P.E., Chung-Sheng Lee,<sup>2</sup> A.M.ASCE, Ph.D., Gilbert A. Hegemier,<sup>3</sup> M.ASCE, Ph.D., Frieder Seible,<sup>4</sup> M.ASCE, Ph.D., P.E.

**Subject headings:** Blast Loads, Concrete Columns, Fiber Reinforced Plastics, Rehabilitation, Full-Scale Tests

## Abstract

Measures to prevent progressive collapse of structures include protection of critical elements such as columns. In support of this goal, nine tests were conducted to assess the as-built performance of typical columns and the effectiveness of carbon fiber jackets in improving their performance. A quasi-static load protocol was developed to replicate in the laboratory the damage patterns observed in blast testing in the field. Load-deflection curves (resistance functions) and jacket strain were measured. Jackets were observed to change the failure mode from brittle shear to ductile flexure and to increase the load and displacement capacities of the column. Variations in jacket strain are discussed and experimental results are used to assess predictive models for shear

---

<sup>1</sup>Instructor, Oregon State University, School of Civil and Construction Engineering, 220 Owen Hall, Corvallis, OR, 97331, rodrigto@enr.orst.edu

<sup>2</sup>Regional Manager, Composite Solutions International, 1455 Research Blvd. Suite 512, Rockville, MD 20850

<sup>3</sup>Professor, University of California, San Diego, Department of Structural Engineering, 9500 Gilman Dr, La Jolla, CA, 92093-0085

<sup>4</sup>Professor, University of California, San Diego, Department of Structural Engineering, 9500 Gilman Dr, La Jolla, CA, 92093-0085

capacity and resistance functions. The data support the use of these models for design but identify some limitations in the resistance functions.

## Introduction

Deliberate explosions targeting critical and high-profile facilities such as the Murrah Federal Building in Oklahoma City underscore the need to protect infrastructure against bomb blasts. As structural engineers our most important task is to protect against progressive collapse, which initiates when a load-bearing member suffers enough damage to lose its load carrying capacity. Once this happens, the failure progresses quickly through the structure if the adjoining elements are not strong enough or if the structure lacks sufficient redundancy or continuity (Malvar 2005; Mohamed 2006). Reinforced concrete (RC) buildings in non-seismic regions are in special danger of progressive collapse because of the combination of large shear demands imposed by blast events and the widely-spaced shear reinforcement in the columns.

Column wraps made from fiber reinforced polymers (FRPs) are a viable hardening technology (Buchan and Chen 2007). FRPs are a composite material made from long, oriented fibers such as glass, carbon, or aramid embedded in a polymer matrix such as an epoxy. FRP structural retrofits of reinforced concrete date from the 1980s (ACI 1996, 2007; Teng et al. 2002), and design approaches are gradually being adopted by governing agencies (ACI 2008; FIB 2001); during this time the authors and collaborators have conducted numerous studies on infrastructure rehabilitation with FRPs, primarily for seismic demands (Hegemier et al. 2007; Seible et al. 2007; Van Den Eindex et al. 2003). FRP column retrofits enhance shear capacity, flexural hinge confinement, flexural capacity, and integrity of lap splices (Priestley et al. 1996; Seible et al.

1997; Teng et al. 2002). They allow the member to deform extensively while maintaining its load bearing capacity. If needed, the strength and stiffness of the member can also be increased to help reduce deflections. FRP retrofits have been successfully implemented in the field.

Additional research needs include more thorough and quantitative results from experimental tests, full descriptions of failure modes, improvements in the accuracy of modeling, and improved design guidelines (Buchan and Chen 2007). This paper contributes, directly or indirectly, to all of these needs. The present results are part of a larger series of studies designed to establish the usefulness of FRP wraps, obtain response data, calibrate computational models, and refine design guidelines (Crawford et al. 2003, 2001; Hegemier et al. 2007, 2003, 2002; Lee 2006; Morrill et al. 2004, 2000, 2001; Seible et al. 2007).

This paper summarizes nine quasi-static tests of as-built and FRP-jacketed RC columns under blast-like loads, detailing the load protocol, observed evolution of damage and failure modes, and measured forces, deflections, and jacket strains. Jacket deformation and modes of failure are discussed and observations are made as to the effectiveness of the FRP jackets in terms of ductility and strength. Comparisons are drawn between experimental data and existing design equations for shear and resistance functions.

## Methods

Experimental work was conducted at the University of California, San Diego (UCSD) Powell Labs. Nine RC column specimens were tested and an additional one was used to develop the loading protocol. The specimens varied primarily in cross sectional dimensions and the thickness of the carbon fiber reinforced polymer (CFRP) wrap. All specimens were of the same height and specified material strengths and were designed with low transverse reinforcement. One specimen had additional, externally-bonded longitudinal CFRP reinforcement and another was free to deform axially. The test matrix in Table 1 summarizes the parameters that were varied across tests.

## Specimen Details

Specimens were typical of mid-rise, non-seismic buildings from the mid-late 20th century. All specimens were 3276 mm tall and had 38 mm of cover concrete to the edge of the stirrups. Cross section dimensions are given in Table 1. Reinforcement was provided as described in Table 2. Minimum specified concrete strength was 34.5 MPa. Averages of three test-day cylinder tests are provided in Table 3. Test-day strength differs between tests because of different time spans between construction and testing; the same concrete mix was specified in all cases and similar behavior is expected for all specimens. Grade 420 reinforcing bar (rebar) was used in both the longitudinal and transverse directions. Three rebar specimens were tested; the average yield stress was 462 MPa and the average ultimate stress was 627 MPa.

The columns were built monolithically with highly-reinforced load stubs and footings at a precasting plant. The composite jackets were applied on site. Prior to the application of CFRP wraps the concrete surface was prepared by sandblasting and the column corners were ground to a 25 mm radius. A concrete surface primer was applied immediately before application of the composite. The CFRP wraps were applied by wet layup over the full height of the column except for 13 mm gaps at the top and bottom to delay direct compression loading of the jacket. The wraps were made from a unidirectional, 610 g/m<sup>2</sup> (18 oz/yd<sup>2</sup>), 406 mm wide fabric with an epoxy resin. After wrapping, the column was tented and the jacket allowed to cure in ambient conditions. Two-ply test panels were prepared and tested according to ASTM D3039-00 (ASTM 2000). The measured properties are summarized in Table 4.

On specimen 14×14×6-st, before the wraps were applied, pultruded Sika CarboDur strips were applied directly to the concrete surface with the Sika Sikadur 30 adhesive. Six strips were applied longitudinally: three on the loaded face and three on the opposite face. A surface primer was applied prior to application of the wraps. Manufacturer properties for the strips are: 100 mm width, 1.2 mm thickness, 165 GPa modulus (mean value), 3100 MPa ultimate tensile stress (mean value), and 1.69% ultimate tensile strain. Each strip was cut to a length of 3251 mm, which is equal to the height of the column minus the 13 mm gaps at top and bottom.

## Test Setup

The test setup (Fig. 1) was designed to replicate the loading and in-situ boundary conditions experienced by an RC moment frame column during blast loading; in a real building the column is preloaded by gravity loads, its ends are fixed due to inertia, and the blast load is applied laterally over the face of the column. Three servo-controlled, closed loop hydraulic actuators were aligned horizontally to apply load to the front face of the column. The center actuator had a capacity of 730 kN and the other two 980 kN. Spreader plates were placed between the actuator and the specimen to apply a uniform load. A 25 mm thick rubber pad was placed between the steel plate and the specimen. Identical plates and pads were used on the back side. The front and back plates were connected with tie rods extending around the outside of the column. The tie rods were not over-tightened and a significant gap was maintained between the column and the tie rods to avoid applying any significant artificial confinement. There was a 38 mm vertical gap between plates. As is explained below, the back plates help impose the deflected shape that is observed after a real blast.

The footing was post-tensioned to the laboratory floor to provide a fixed restraint. A concrete block behind the footing transferred shear forces to the strong wall. The load stub at the top of the column was restrained by a link system that provided moment and lateral fixity while allowing unrestrained vertical motion. The link system was post-tensioned to the load stub and reaction wall by hydraulic jacks. Although perfect fixity was sought, this

support was in reality only partially fixed. Vertical load was imposed by two 980 kN capacity, servo-controlled, closed-loop hydraulic actuators at either side of the specimen. The actuators applied load to a steel cross beam that was bolted to the load stub by a connection designed to withstand both tension and compression. Once the load was applied, the actuators were held in place to provide vertical fixity (during a blast event inertial effects render the boundary conditions fixed despite the flexibility of the adjoining structural elements).

Instrumentation was provided to measure forces and displacements in all actuators, transverse strains on the FRP jackets, and lateral specimen displacements. The location at which strain was measured differed from test to test.

## **Loading Protocol**

The principal objective in defining the loading protocol was to replicate the deflected shape observed in field tests. It was hypothesized that by matching shapes, the observed damage progression, failure modes, and load-deflection curves would be most representative of field conditions. In field tests, RC columns with poor shear reinforcement suffer significant shear deformation at the ends and minor flexural deformation at midspan (Fig. 2a). To enforce this behavior in the laboratory, steel plates were placed at the back of the specimens and were tied with post-tensioning rods to the spreader plates at the actuators. Lateral load was applied quasi-statically with the center actuator in displacement control and the other two actuators matching the force in the



center actuator, resulting in a uniform load on the column. Candidate load protocols were tried on a sacrificial as-built specimen. Based on the results, the following load protocol was followed on subsequent tests: (1) Apply a vertical load of 445 kN to simulate the in-situ axial load on the column. Once the load is applied, hold the vertical actuators in place by closed-loop control. (2) Load the specimen quasi-statically to failure or to the maximum displacement capacity of the test setup. The protocol originally specified unloading the specimen once it reached a target load so the back plates could be removed. Due to accidental actuator slippage in test 6, this step was omitted in the remaining tests.

## Results

### Overview of Response

In Fig. 3 lateral and vertical load envelopes are plotted against lateral deflection at mid-height (or simply “deflection”). Table 5 details the maximum lateral and vertical loads ( $R_{uc,l}$  and  $R_{uc,v}$ , respectively), the deflections at which they occur ( $x_{uc,l}$  and  $x_{uc,v}$ ), and the ultimate deflection ( $x_{\max}$ , defined as the deflection at which the load has dropped to 80% of the maximum load). Raw data (Hegemier et al. 2003, 2002) were corrected to remove the effects of excessive flexibility in the top restraint at the start of loading (caused by gaps in the pin connections). Data from test 14×14×6-st required an additional correction due to the accidental slippage of an actuator.

The as-built columns failed by the formation of diagonal shear cracks oriented between  $25^\circ$  and  $35^\circ$  from vertical. Greater flexibility in the top restraint caused shear cracking (and eventual failure) to initiate first at the base of the column and later at the top, except for the  $12 \times 12$  specimen, which did not fail at the top. At shear failure there was a large and sudden drop in both the lateral and vertical loads. In the axially restrained columns the axial force decreased significantly after shear failure, even becoming tensile in the  $14 \times 14$  specimen. In a residual axial capacity test, specimen  $14 \times 14 \times 0$  reached 350 kN (only 78% of the in-situ axial load) and suffered significant lateral, second-order deflections. Post-test photographs of the specimens (Fig. 2b) show the characteristic displaced shape with deformation concentrated in shear at the top and bottom.

The jacketed specimens behaved in a ductile manner, with the level of ductility dependent on the thickness of the jacket. As lateral deflection increased, flexural hinges occurred first at the column ends and then at mid-height (Fig. 2c). The jacket suffered horizontal flexural cracking between the fibers and matrix. Yielding of reinforcing bars occurred in the footing and load stub. A jacket section removed from one specimen after testing revealed relatively undamaged concrete with thin cracks between  $25^\circ$  and  $35^\circ$  from vertical.

The  $14 \times 14 \times 2$  and  $14 \times 14 \times 4$  specimens failed when FRP ruptured at the base of the column, on the compression side at one of the rounded corners. After failure, the lateral and vertical loads dropped suddenly. The other columns

did not fail catastrophically although local signs of distress such as yielding rebar, local jacket bucking, and local jacket rupture were observed. The rectangular columns exhibited greater post-peak strength reduction than the square columns. In the specimen with longitudinal FRP the lateral load peaked early and then dropped suddenly shortly afterward due to failure of longitudinal FRP. After this, the behavior was ductile with a higher residual strength than the other  $14\times 14$  columns. Residual axial capacity tests were performed on specimens  $14\times 14\times 2$ ,  $\times 4$ ,  $\times 6$ , and  $18\times 12\times 3$ -sa; all specimens resisted at least 1030 kN (230% of the in-situ load) without failure.

## **Jacket Behavior**

FRP jackets were instrumented to measure variations in jacket transverse strain over the column height and around the perimeter. All specimens had gauges applied to the center of each side in 152 mm increments up to 914 mm from the base. In tests 2 and 3 gauges were applied in similar locations at the top. In subsequent tests, strain at the top was not measured to allow for more instrumentation at the base. In tests 6 and 10, gauges were applied 152 mm, 305 mm, and 457 mm from the base at all corners and at the center of all four sides. In tests 8 and 9, gauges were applied 76 mm, 152 mm, 305 mm, and 457 mm from the base at all corners and at quarter points of all four sides.

Representative results from the column sides are shown in Fig. 4. At equal lateral displacement, strains measured in the specimen with a two-ply composite jacket were higher than those in the specimen with a six-ply jacket;

strains in specimen with a four-ply jacket (not shown) were in between the two. In general, strain was seen to increase closer to the footing except right next to the footing where it decreased again due to boundary effects. Behavior at the top was similar but less pronounced. The largest strain recorded in all specimens at the center of the column side was  $7.2 \text{ m}\epsilon$ , well below rupture strain reported in Table 4.

A representative example of strain variation around the perimeter is shown in Fig. 5. Strains are nearly symmetric about the centerline and higher on the compression side of the column because of dilatancy of concrete in compression. Strains measured at the corners are lower than strains on the sides and can even become negative (compressive). Strains as low as  $-15.1 \text{ m}\epsilon$  were recorded. This phenomenon is discussed below.

## Discussion

### Behavior of CFRP Jacket

All jacketed specimens formed a ductile, plastic hinge mechanism instead of failing in brittle shear. As a result both displacement capacity and strength of the jacketed specimens increased significantly over the as-built specimens. The deflection at failure of specimens  $14 \times 14 \times 2$  and  $\times 4$  was 5.0 and 7.2 times greater than that of the as-built specimen. Specimen  $14 \times 14 \times 6$ -st sustained deflections 10.0 times greater without failing. The strength of the jacketed  $14 \times 14$  specimens (without longitudinal FRP) was between 1.7 and 1.8 times

the unretrofitted specimen. The longitudinal, surface-bonded FRP provided an additional strength gain at the expense of early maximum strength. These increases in strength and ductility capacity improve the energy absorption capacity of the column and reduce deflections; the reduced deflections in turn reduce the risk of geometric instabilities that can lead to progressive collapse. It is important to note that despite failing laterally the column can have enough residual axial capacity to support the in-situ axial load. This is both because the jacket remains functional in providing axial confinement and because the jacket preserves the integrity of the concrete core during lateral loading.

Turning to jacket strains, we note that while strains are expected to vary through the jacket thickness, they were measured only on the surface. Nonetheless, higher ductilities in specimens with thicker jackets are easily explained by lower jacket strains at similar displacement levels. The decrease in strain close to the column ends can be explained by the confinement provided by the footing and load stub. In the specimens that failed by jacket rupture, the measured strains at failure were lower than the measured rupture strain of the material. Three reasons contribute to this discrepancy: (1) the low probability of recording strain exactly at the location of failure, (2) biaxial loading of the jacket compared with uniaxial loading of test coupons, and (3) reductions in surface strain due to bending deformations at the corners (Cole and Belarbi 2001; Fam et al. 2005). Bending deformation at the corners occurs because the jacket provides less confinement along the edge than at the corner. The concrete at the edges dilates more and places the corner in flexure with a

compressive strain at the surface.

## Shear Capacity

The UCSD shear model for columns (Priestley et al. 1996 with enhancements by Kowalsky and Priestley 2000) has been recognized as providing the best correlation with experimental data, most recently by Elsanadedy and Haroun (2005). The model includes contributions from concrete ( $V_c = k\sqrt{f'_c}(0.8A_g)$ ), steel ( $V_s = A_v f_y D' \cot \theta / s$ ), axial load ( $V_p = P \tan \alpha$ ), and FRP ( $V_f = 2t_j f_f h \cot \theta$ ). The factor  $k$  accounts for shear degradation in the plastic hinge and depends on aspect ratio, longitudinal reinforcement ratio, and displacement ductility.  $A_g$  is the gross cross sectional area,  $f'_c$  the compressive strength of concrete,  $A_v$  the area of steel shear reinforcement,  $f_y$  the yield stress of steel,  $D'$  the depth of the concrete core measured from center of transverse reinforcement,  $\theta$  the shear crack angle,  $s$  the spacing of transverse reinforcement,  $P$  the axial load,  $\alpha$  the angle formed between the column axis and the diagonal compression strut,  $t_j$  the thickness of the jacket,  $f_f$  the rupture stress of FRP, and  $h$  the section depth. The model is developed with a shear crack angle of  $30^\circ$ , which is consistent with the crack angle observed in our tests. The axial load contribution, not included in other shear models, recognizes that there is a lateral component to the force developed in the compression struts. In this study the compression strut is assumed to run from the center of the compression zone at the top of the column to the center of the compression zone at mid-height, i.e.,  $\tan \alpha = (h - c)/(2L)$ , where  $c$  is the neutral axis depth

and  $L$  the column length.

Shear capacity was calculated with this model using the appropriate specimen details and measured material strengths. Since lateral force is resisted at both the top and bottom of the column the total nominal shear capacity is  $2 \cdot (V_c + V_s + V_p + V_f)$ . This shear model was developed for a constant axial load. For this reason, although the axial load can vary during a blast, the shear calculations were made with a constant axial load equal to the initial load. Retrofitted columns were calculated to have a shear capacity far exceeding the maximum demand (consistent with flexural failure observed in these specimens). The as-built columns failed by shear and provide useful data to compare with the model. Predicted capacities were 796 kN for specimen 14×14×0 (5.3% error), 695 kN for specimen 14×14×0-ax (5.9% error), and 458 kN for specimen 12×12×0 (-4.2% error). Although this is in good agreement, it is of interest for future studies to consider how to best account for the varying axial load.

## **Resistance Functions**

The axial constraint introduces two additional resistance mechanisms besides flexure: arch action (also called compression membrane), whereby compression struts create a shallow arch resisting lateral displacement, and catenary action (also called tension membrane), whereby the steel reinforcement deforms sufficiently to act as if it were a cable. These effects are recognized in UFC 3-340-01 (DoD 2002) but not UFC 3-340-02 (DoD 2008).

The two as-built 14×14 tests demonstrate the influence of the axial restraint on as-built columns. The maximum load of the axially restrained column was 1.15 times larger than that of the axially free column. This small increase is likely due to arch action. The shear failure caused an immediate loss of arch action. After this, with increased deflection, a tension membrane began to form causing a two-fold difference in residual force by the end of the as-built 14×14 tests (had the test continued, this difference would have increased). Tension membrane action is of low importance because it occurs at large deflections; by the time any significant tension membrane is formed, the column has sustained enough residual deflection that it will fail under subsequent axial load. This conclusion is supported by the residual axial capacity test conducted on specimen 14×14×0, in which the axial capacity was insufficient to carry the in-situ gravity load.

Turning to the retrofitted specimens one can compare test results to theoretical resistance functions. Resistance functions describe the quasi-static resistance of the specimen per unit length as a function of midheight deflection. To account for dynamic effects these resistance functions would be subsequently modified by a dynamic increase factor. In this paper, the theoretical resistance functions are multiplied by the column length to compare directly with measured load-deflection curves. Theoretical resistance functions are determined in the following way as recommended by UFC 3-340-01 and UFC 3-340-02:

1. The initial behavior is determined by the formation of a plastic flexural



mechanism.

- (a) A column with fixed ends and subjected to a lateral uniform load will first develop plastic hinges at both ends at a resistance  $R_e = 12M_e/L$  and initial stiffness  $K_e = 384EI/L^3$ , where  $M_e$  is the moment capacity at the column ends,  $L$  the column length and  $EI$  the flexural stiffness. The deflection at  $R_e$  is  $x_e = K_e R_e$ .
- (b) Stiffness after formation of the first plastic hinges is  $K_{ep} = 384EI/5L^3$ . With an increase in load the column will form a final hinge at midspan at a resistance  $R_u = 8(M_e + M_c)/L$ , where  $M_c$  is the moment capacity at the center. The deflection at  $R_u$  is  $x_p = x_e + (R_u - R_e)K_{ep}$ .

Equations for other boundary conditions are similar. UCF-3-340-02 suggests using an effective moment of inertia equal to the average of the gross and cracked moments of inertia ( $I_e = (I_g + I_{cr})/2$ ).

2. After formation of a flexural mechanism, load increases to the ultimate arch resistance, which was derived by Park and Gamble (1980) based on the mechanism formed in a beam loaded by one or two point loads. The total lateral load resisted by arch action ( $R_{uc}$ ) is given by Park's and Gamble's equations (too long to reproduce here) evaluated at a deflection  $x_{uc}$  (discussed below). Since these equations consider only a top and bottom layer of steel, arch action in our specimens was calculated with all the tension steel lumped into a single layer. The deflection  $x_{uc}$

is calculated with the equation from UCF-3-340-01, which depends on column height  $L$  and depth  $h$ . For all columns in this study,  $x_{uc}$  is 109 mm.

3. After the peak, the resistance function decreases linearly to a residual resistance. For a well-confined FRP-jacketed column, the residual resistance is based on the original moment capacities (in other cases loss of cover concrete would be considered). After this, the resistance function would rise due to tension membrane, but our retrofitted specimens did not reach this regime of behavior. Details can be found in UCF-3-340-01.

Theoretical and experimental curves are compared in Fig. 6. Because of the partial fixity in the top support of the experimental setup, each test is plotted against two predictions: a column with fixed ends and one with a fixed base and pinned top. The resistance functions were calculated according to the above procedure using measured material properties. Theoretical curves are plotted up to the maximum deflection in the corresponding experimental test; prediction of the deflection at failure is beyond the scope of this paper. Moment-curvature behavior was found from the Response-2000 computer program (Bentz 2001) with the initial axial load of 445 kN imposed throughout the analysis. Concrete confinement was not considered.

The specimen with longitudinal strips required special treatment. The longitudinal strips increase moment capacity at the center, but not at the ends because they lack adequate development length. The moment at the center was computed by moment-curvature analysis with the capacity of the

strips governed by debonding. The stress in the strip at debonding is  $\sigma_{db} = 1.1 \cdot 0.707 \cdot \sqrt{E_f \sqrt{f'_c}/t_f}$  in MPa and mm, where  $E_f$  is the modulus of the strips and  $t_f$  their thickness (Teng et al. 2002). This results in a capacity for the strip of 792 MPa (far lower than the rupture stress) and a corresponding strain to failure of 0.480%. After debonding of the strips, the moment capacity at the center reverts to the value without strips. For computing arch action resistance it was necessary to treat the FRP as an equivalent area of steel in the same lumped layer as the reinforcing steel. To predict the deflection at which debonding occurred, the curvature at debonding ( $\phi_{db}$ ) was obtained from the moment-curvature calculation and the plastic hinge length was assumed to be equal to the depth of the column ( $h$ ). From a three hinge mechanism the deflection at debonding is thus  $(L/2) \tan(h \cdot \phi_{db})$ .

The initial stiffness of the predicted curves is too large. This is believed to be in large part because the effective moment of inertia was taken as the average of gross and cracked moments of inertia. To explore this conclusion the analysis was repeated using the equation adopted by the American Concrete Institute (ACI) for effective moment of inertia:  $I_e = I_g(M_{cr}c/M_a)^3 + I_c(1 - (M_{cr}/M_a)^3)$ , where  $I_g$  is the gross moment of inertia,  $I_c$  is the cracked moment of inertia,  $M_{cr}$  is the cracking moment, and  $M_a$  is the applied moment (ACI 2005). Calculations using the ACI equation provide better agreement, with the experimental curves approximating the fixed-pinned prediction. The change in moment capacity due to the variation in axial load has also been investigated in a preliminary manner and shown to have a smaller effect on the predictions

than the effective moment of inertia. Modeling these phenomena in a way appropriate for design is an interesting topic for future studies.

Near the peak, resistance ( $R_{uc}$ ) is generally estimated much better than the displacement at peak resistance ( $x_{uc}$ ). The predicted value of  $x_{uc}$  is compared to recorded values of deflection at peak lateral load ( $x_{uc,l}$ ) and deflection at peak vertical load ( $x_{uc,v}$ ) in Table 6. The theoretical value overestimates all experimental values. For the square columns, the recorded deflection is on average 80% of theoretical; it ranges between 71% and 87%. Agreement for non-square columns was worse;  $x_{uc,l}$ , which is most appropriate to compare to  $x_{uc}$ , was at best 60% of theoretical. The ratio of  $x_{uc,v}$  to  $x_{uc}$  was better in both cases although the meaning of this is not clear since  $x_{uc}$  should be related to measured displacement at maximum lateral (not vertical) load. These results indicate that the equation for  $x_{uc}$  should be used with caution, especially with non-square columns.

At medium to large deflections, the measured curves for the 14×14 columns without strips lie completely between the two calculations. The match for non-square columns is not as good. This seems to be driven by the worse agreement for  $x_{uc}$  in these cases. The curves for the 14×14 column with strips also lies between the two estimates. It does not, however, display the same ascending and descending behavior of the predictions.

In summary, although specific areas of improvement have been identified in the theoretical resistance functions, considering the high variability expected from other inputs to the design process (e.g., charge size, type, and standoff), it

is concluded that the theoretical resistance functions are adequate as a means of obtaining estimates of load-deflection behavior for design purposes.

## Summary and Conclusions

Nine rectangular RC specimens with and without FRP jackets were tested under quasi-static blast-like loading. One of the jackets had fibers oriented along the transverse and longitudinal directions; the rest were transverse-only. A load protocol was developed to replicate in the laboratory the damage patterns observed in the field. Load-deflection curves (resistance functions) and surface jacket strains were recorded. The specimens with FRP jackets were observed to form ductile three-hinge mechanisms while those without jackets failed suddenly in shear. Specimens with thicker jackets developed a greater ductility and lower jacket strains. Variations in strain in the transverse and longitudinal directions were discussed. The experimental results were used to assess the UCSD shear model and standard guidance for resistance functions contained in UFC 3-340-01. Limitations in both approaches are identified. The UCSD shear model performed well. It was argued that when keeping in mind the large uncertainty in other design inputs the resistance functions are adequate for design.

## Acknowledgements

This work was funded by the Defense Threat Reduction Agency (DTRA). Don Phillippi provided useful editorial comments. Andrew Budeck and Ludger Dieckmann contributed to discussions and analysis in early phases of the project. Chris Latham was instrumental in developing the loading scheme.

## Notation

*The following symbols are used in this paper:*

$A_g$  = Gross cross sectional area

$A_v$  = Area of shear steel reinforcement

$c$  = Neutral axis depth

$D'$  = Depth of concrete core measured from center of transverse reinforcement

$E_f$  = Modulus of longitudinal FRP strips

$EI$  = Flexural stiffness

$f'_c$  = Compressive strength of concrete

$f_f$  = Rupture stress of FRP

$f_y$  = Yield stress of steel

$h$  = Depth of column (dimension parallel to loading direction)

$I_c$  = Cracked moment of inertia

$I_e$  = Effective moment of inertia

$I_g$  = Gross moment of inertia

$k$  = Scaling factor used with  $V_c$

$K_e$  = Initial elastic stiffness of resistance function  
 $K_{ep}$  = Secondary elastoplastic stiffness of resistance function  
 $L$  = Column height  
 $M_a$  = Applied moment (to calculate effective moment of inertia)  
 $M_{cr}$  = Cracking moment  
 $M_e$  = Moment capacity at the end of the column  
 $M_c$  = Moment capacity at the center of the column  
 $P$  = Axial load used for calculating shear capacity  
 $R_e$  = Resistance at the end of elastic behavior  
 $R_u$  = Resistance at formation of a plastic mechanism  
 $R_{uc}$  = Maximum theoretical arch action resistance  
 $R_{uc,l}$  = Maximum recorded lateral load  
 $R_{uc,v}$  = Maximum recorded vertical load  
 $s$  = Spacing of transverse reinforcement  
 $t_f$  = Thickness of longitudinal FRP strips  
 $t_j$  = Thickness of FRP jacket  
 $V_c$  = Contribution of concrete to shear resistance  
 $V_f$  = Contribution of FRP to shear resistance  
 $V_p$  = Contribution of axial load to shear resistance  
 $V_s$  = Contribution of steel to shear resistance  
 $x_e$  = Deflection at end of elastic behavior  
 $x_p$  = Deflection at formation of a plastic mechanism  
 $x_{uc}$  = Theoretical deflection at maximum arch action resistance

$x_{uc,l}$  = Deflection at maximum recorded lateral load

$x_{uc,v}$  = Deflection at maximum recorded vertical load

$x_{\max}$  = Maximum recorded deflection

$\alpha$  = Angle from vertical formed by diagonal compression strut

$\phi_{db}$  = Curvature at which debonding occurs

$\sigma_{db}$  = Debonding stress of longitudinal FRP strips

$\theta$  = Shear crack angle



# Tables

Table 1: Test Matrix

Test No.	Test Designation	Cross Section [mm×mm]	No. of Wraps	Note
4	14×14×0	356 × 356	0	
5	14×14×0-ax	356 × 356	0	No axial load
2	14×14×2	356 × 356	2	
10	14×14×4	356 × 356	4	
3	14×14×6	356 × 356	6	
6	14×14×6-st	356 × 356	6	Longit. strips
7	12×12×0	305 × 305	0	
8	12×18×3-sa	305 × 457	3	Strong axis
9	18×12×3-wa	457 × 305	3	Weak axis

Note: Test designation specifies width and depth in inches, number of wraps, and a note if needed. Test number is chronological.

Table 2: Specimen Reinforcement

Designation	Longitudinal		Transverse (#10)	
	Bars	Ratio	Spacing	Ratio
14×14 (all)	8 #25	3.24%	324 mm	0.12%
12×12×0	4 #19	1.23%	305 mm	0.15%
12×18×3-sa	6 #19	1.23%	305 mm	0.15%
18×12×3-wa	6 #19	1.23%	305 mm	0.10%

Notes: Metric bar designation used. Ratio is steel area divided by corresponding gross concrete area.

Table 3: Measured Concrete Strength (day of test)

Designation	Strength [MPa]
14×14×0	38.7
14×14×0-ax	43.9
14×14×2	38.9
14×14×4	48.3
14×14×6	37.6
14×14×6-st	56.9
12×12×0	37.0
12×18×3-sa	36.8
18×12×3-wa	35.9

Table 4: Measured Composite Properties

Designation	Rupture Stress [MPa]	Rupture Strain [%]	Modulus [MPa]	Thickness [mm]
14×14×2	848	1.12	73.8	2.14
14×14×4	924	1.15	75.1	4.11
14×14×6	848	1.12	73.8	6.42
12×18×3-sa	814	1.01	75.8	2.93
18×12×3-wa	814	1.01	75.8	2.93

Notes: Total jacket thickness calculated from measured thickness of two-ply test specimen. Data for 14×14×6-st suggest that the test sample was too dry; the values for 14×14×6 were used instead.

Table 5: Peak Values from Load-Deflection Curves

Designation	$R_{uc,l}$	$x_{uc,l}$	$R_{uc,v}$	$x_{uc,v}$	$x_{\max}$
14×14×0	756	18	762	18	23
14×14×0-ax	657	20	-	-	27
14×14×2	1302	83	1287	78	115
14×14×4	1329	85	1475	87	165
14×14×6	1389	94	1427	95	-
14×14×6-st	1608	57	1608	95	-
12×12×0	478	25	815	27	28
12×18×3-sa	1379	66	1717	82	185
18×12×3-wa	815	59	1617	102	139

Note: Forces ( $R$ ) in kN, deflections ( $x$ ) in mm

Table 6: Deflection of retrofitted columns at maximum load

Column	$x_{uc,l}/x_{uc}$	$x_{uc,v}/x_{uc}$
Square columns (average)	0.80	0.81
12×18×3-sa	0.60	0.75
18×12×3-wa	0.54	0.93

# Figures

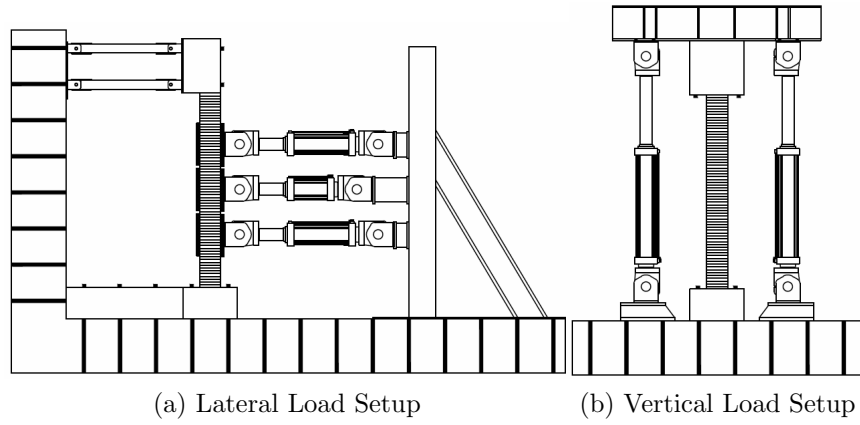


Figure 1: Elevations of Test Setup

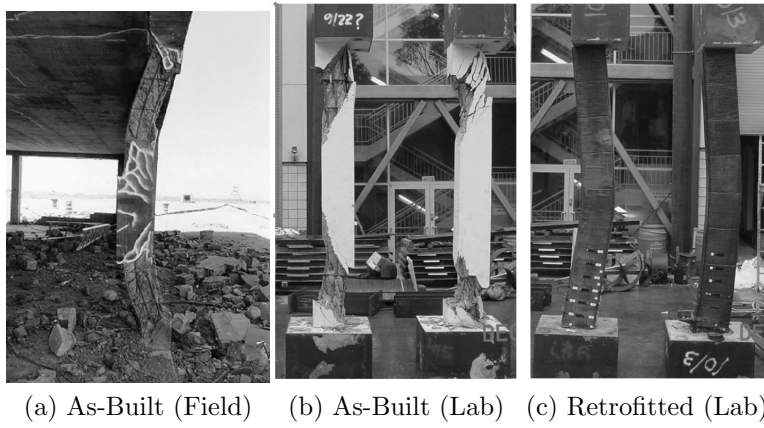
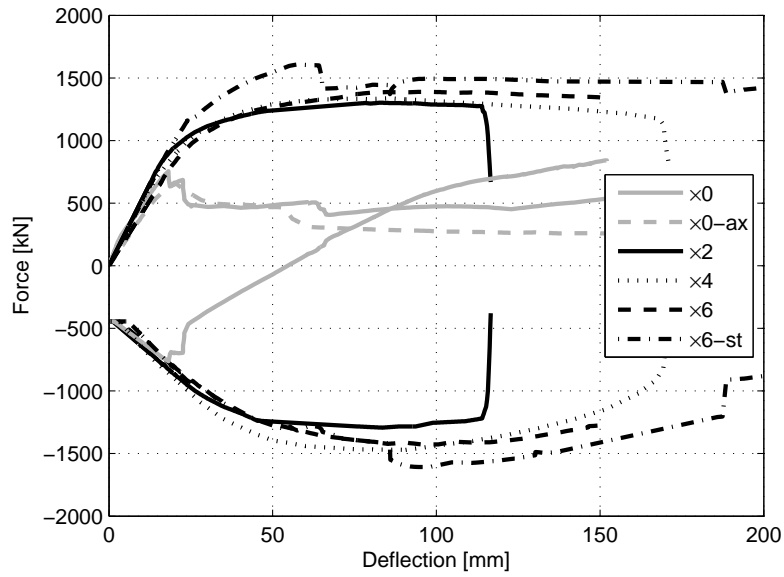
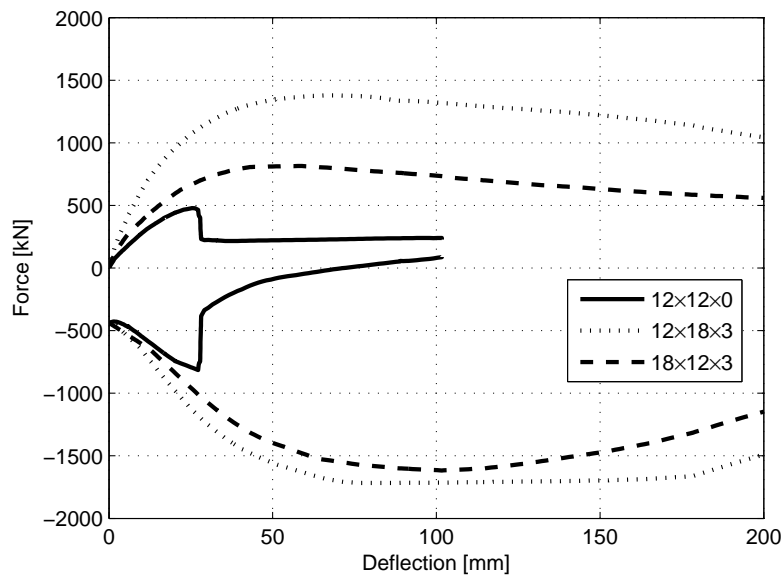


Figure 2: Specimens After Testing

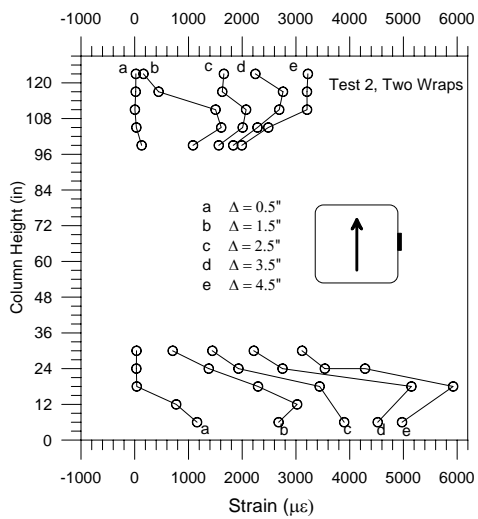


(a) 14×14 Specimens

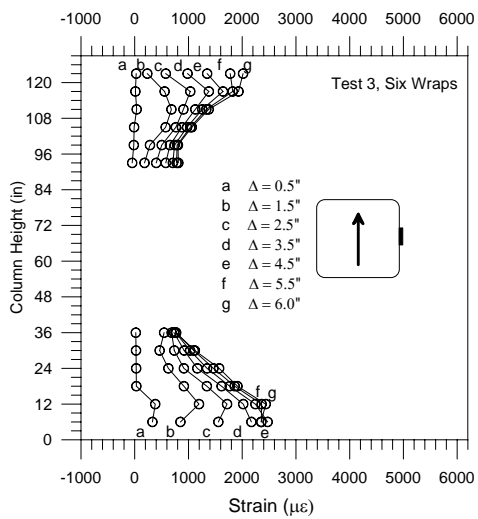


(b) Other Specimens

Figure 3: Load-Deflection Curves (Axial Load is Negative in Compression)



(a)  $14 \times 14 \times 2$



(b)  $14 \times 14 \times 6$

Figure 4: Variation of Transverse Jacket Strains along Column Height (1" = 25.4 mm)

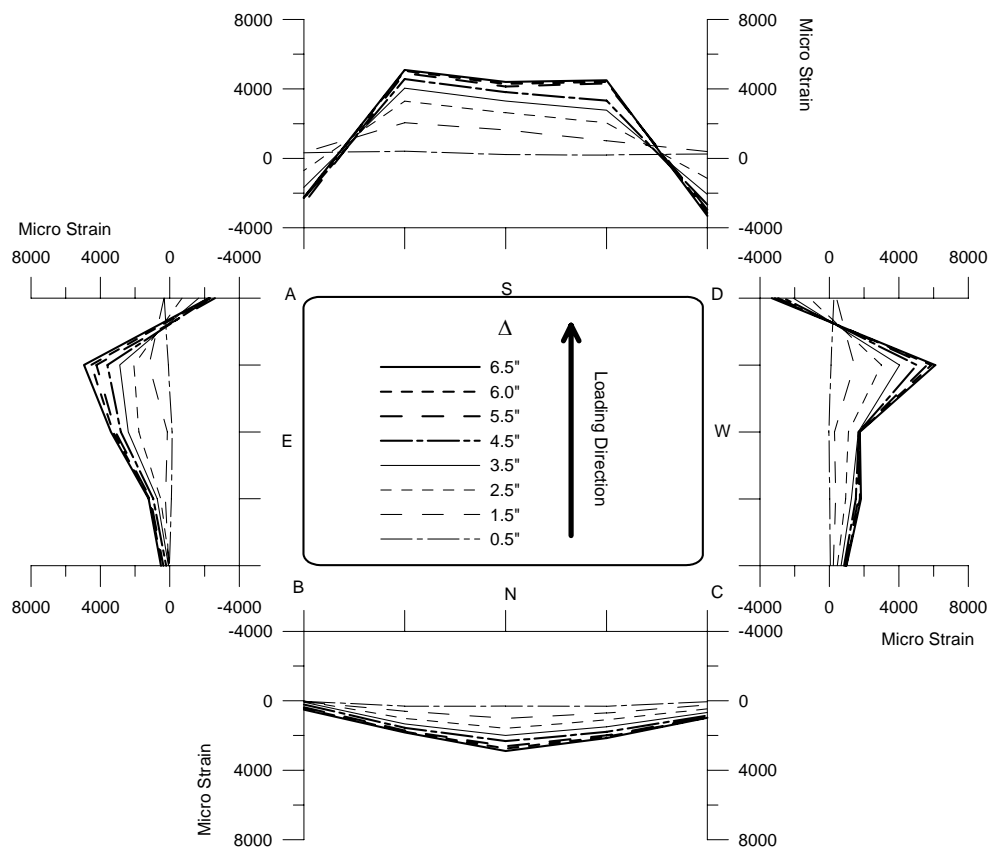


Figure 5: Transverse Strain Profiles, Test 18×12×3-wa at 76 mm height (1" = 25.4 mm)

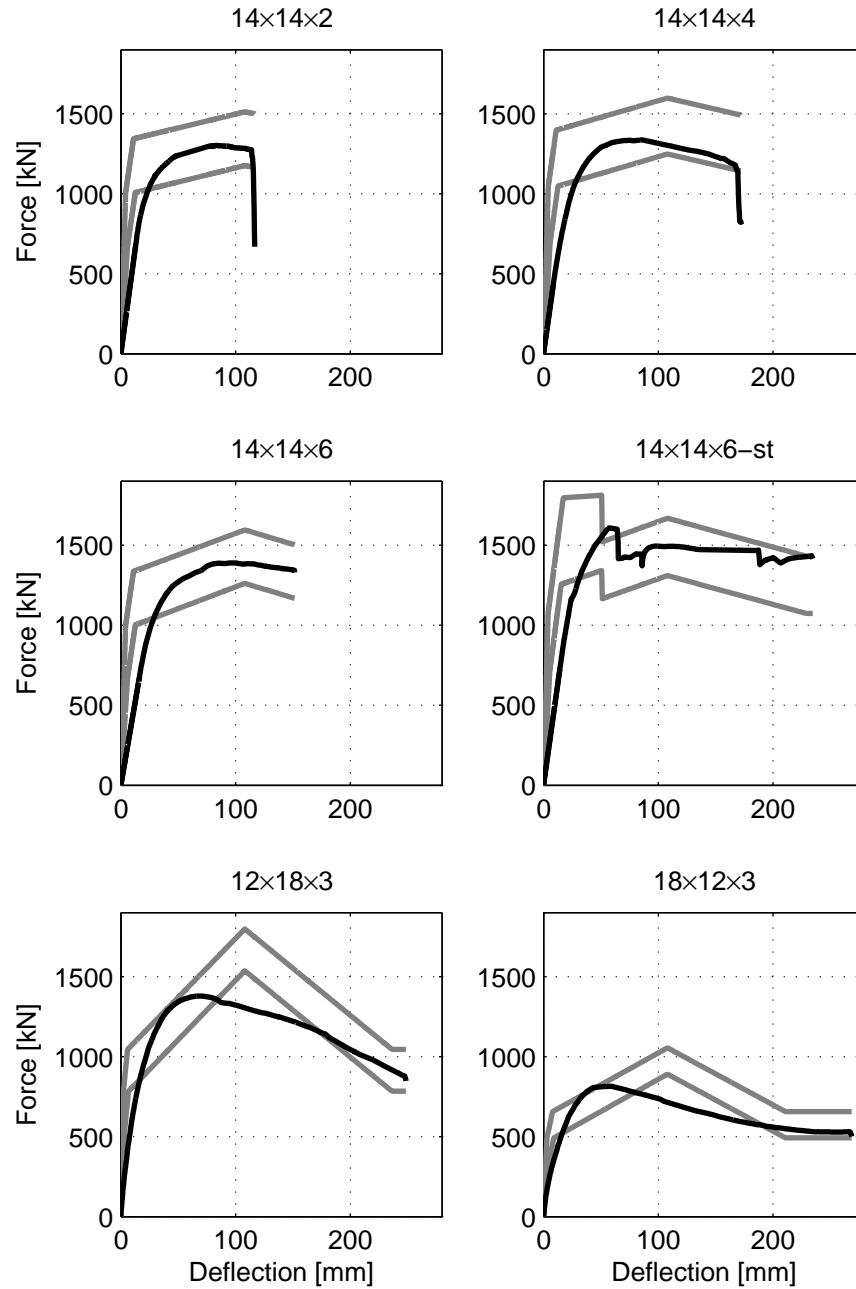


Figure 6: Resistance Functions (Jacketed Specimens), Measured (Black) and Calculated (Grey, Upper = Fixed-Fixed, Lower = Fixed-Pinned)



## References

- ACI (1996). *State-of-the-Art Report on Fiber Reinforced Plastic (FRP) Reinforcement for Concrete Structures*. ACI 440R-96 (Reapproved 2002), American Concrete Institute.
- ACI (2005). *Building Code Requirements for Structural Concrete and Commentary*. ACI 318-05, American Concrete Institute.
- ACI (2007). *Report on Fiber-Reinforced Polymer (FRP) Reinforcement for Concrete Structures*. ACI 440R-07, American Concrete Institute.
- ACI (2008). *Guide for the Design and Construction of Externally Bonded FRP Systems for Strengthening Concrete Structures*. ACI 440.2R-08, American Concrete Institute.
- ASTM (2000). “Standard test method for tensile properties of polymer matrix composite materials.” *ASTM Test Standard D 3039-00*, ASTM International, West Conshohocken, PA.
- Bentz, E. (2001). *Response-2000, Shell-2000, Triax-2000, Membrane-2000 User Manual*. <<http://www.ecf.utoronto.ca/~bentz/manual2/final.pdf>> as of 29 Sep 2010.
- Buchan, P. and Chen, J. (2007). “Blast resistance of FRP composites and polymer strengthened concrete and masonry structures – A state-of-the-art review.” *Composites: Part B*, 38(5–6), 509–522.

- Cole, C. and Belarbi, A. (2001). “FRP jacketed reinforced concrete columns.” *CIES 99-13*, Center for Infrastructure Engineering Studies, UM-Rolla.
- Crawford, J. E., Malvar, L. J., Ferritto, J. M., Morrill, K. B., Dunn, B. W., and Bong, P. (2003). “Description of design software for retrofitting reinforced concrete columns to improve their resistance to blast.” *Report TR-01-16.3*, Karagozian & Case, Burbank, CA, USA. Limited Distribution.
- Crawford, J. E., Malvar, L. J., Morrill, K. B., and Ferritto, J. M. (2001). “Composite retrofits to increase the blast resistance of buildings.” *10th International Symposium on Interaction of the Effects of Munitions with Structures*, San Diego, CA, USA.
- Elsanadedy, H. M. and Haroun, M. A. (2005). “Seismic design guidelines for squat composite-jacketed circular and rectangular reinforced concrete bridge columns.” *ACI Structural Journal*, 102(4), 505–514.
- Fam, A., Schnerch, D., and Rizkalla, S. (2005). “Rectangular filament-wound glass fiber reinforced polymer tubes with concrete under flexural and axial loading: Experimental investigation.” *Journal of Composites for Construction*, 9(1), 25–33.
- FIB (2001). *Externally bonded FRP reinforcement for RC structures*. Fédération Internationale du Béton, Laussane, Switzerland.
- Hegemier, G., Seible, F., Karbhari, V., Lee, C., Rodriguez-Nikl, T., Oesterle, M., Morrill, K., and Crawford, J. (2007). “The use of fiber reinforced poly-

- mers to mitigate natural and man-made hazards.” *8th International Symposium on Fiber Reinforced Polymer Reinforcement for Concrete Structures (FRPRCS-8)*, Patras, Greece.
- Hegemier, G. A., Seible, F., Lee, C.-S., and Rodriguez-Nikl, T. (2003). “FRP-based blast retrofit design strategies - Laboratory tests on rectangular RC columns - Part II.” *Research Report SSRP-2002/17*, UCSD Structural Engineering, La Jolla, CA, USA. Limited Distribution.
- Hegemier, G. A., Seible, F., Rodriguez-Nikl, T., Lee, C.-S., Budek, A. M., and Dieckmann, L. (2002). “FRP-based blast retrofit design strategies - Laboratory tests on rectangular RC columns.” *Research Report SSRP-2002/04*, UCSD Structural Engineering, La Jolla, CA, USA. Limited Distribution.
- Kowalsky, M. J. and Priestley, M. J. N. (2000). “Improved analytical model for shear strength fo circular reinforced concrete columns in seismic regions.” *ACI Structural Journal*, 97(3), 388–396.
- Lee, C.-S. (2006). “Modeling of FRP-jacketed RC columns subject to combined axial and lateral loads,” PhD thesis, University of California, San Diego.
- Malvar, L. (2005). “Specific local resistance concepts.” *Concrete International*, 27(12), 23–27.
- Mohamed, O. A. (2006). “Progressive collapse of structures: Annotated bibliography and comparison of codes and standards.” *Journal of Performance of Constructed Facilities*, 20(4), 418–425.

- Morrill, K., Malvar, L., Crawford, J., and Ferritto, J. (2004). "Blast resistant design and retrofit of reinforced concrete columns and walls." *2004 Structures Congress*, American Society of Civil Engineers.
- Morrill, K. B., Malvar, L. J., Crawford, J. E., and Attaway, S. (2000). "RC column and slab retrofits to survive blast loads." *2000 Structures Congress*, American Society of Civil Engineers.
- Morrill, K. B., Malvar, L. J., Crawford, J. E., Hegemier, G., and Seible, F. (2001). "Full-scale testing of reinforced concrete column retrofits to resist blast loads." *Proceedings of the 10th International Symposium on Interaction of the Effects of Munitions with Structures*, San Diego, CA, USA.
- Park, R. and Gamble, W. L. (1980). *Reinforced Concrete Slabs*. John Wiley & Sons.
- Priestley, M. J. N., Seible, F., and Calvi, G. M. (1996). *Seismic Design and Retrofit of Bridges*. John Wiley & Sons.
- Seible, F., Hegemier, G., Karbhari, V., Lee, C.-S., Rodriguez-Nikl, T., Oesterle, M., Hutchinson, T., Morrill, K., and Crawford, J. (2007). "Mitigation of natural and man-made hazards in our constructed environment." *4. Symposium Experimentelle Untersuchungen von Baukonstruktionen*, Institut Für Massivbau, Technische Universität Dresden, Dresden, Germany.
- Seible, F., Priestley, M. J. N., Hegemier, G. A., and Innamorato, D. (1997). "Seismic retrofit of RC columns with continuous carbon fiber jackets." *Journal of Composites for Construction*, 1(2), 52–62.

- Teng, J. G., Chen, J. F., Smith, S. T., and Lam, L. (2002). *FRP Strengthened RC Structures*. John Wiley & Sons.
- DoD (2002). *Design and Analysis of Hardened Structures to Conventional Weapons Effects*. UFC 3-340-01, U.S. Department of Defense. Limited Distribution.
- DoD (2008). *Structures to Resist the Effects of Accidental Explosions*. UFC 3-340-02, U.S. Department of Defense.
- Van Den Eijnde, L., Zhao, L., and Seible, F. (2003). “Use of FRP composites in civil structural applications.” *Construction and Building Materials*, 17, 389–403.